MicroBooNE Public Note

Measurement of Neutral-Current π^0 Cross Section in MicroBooNE using Wire-Cell Reconstruction

The MicroBooNE Collaboration

May 30, 2022

Abstract

This note presents the extraction of flux-averaged total and differential neutral-current π^0 cross section measurements, based on the Wiener-SVD unfolding method, using the MicroBooNE Liquid Argon Time Projection Chamber (LArTPC) and the Wire-Cell reconstruction paradigm. This measurement is critical for single-photon searches as neutral-current pion production represents one of the largest sources of background. We report the results for an exposure corresponding to 5.327×10^{19} protons-on-target (POT).

MICROBOONE-NOTE-1111-PUB

MICROBOONE_INFO@fnal.gov

Contents

1 Introduction and Motivation

In this note we report measurements of inclusive neutral-current neutral pion (NCπ^0) flux-averaged total and differential cross sections in MicroBooNE [1] for a statistically limited data set ($\sim 5.327 \times 10^{19}$ POT). The full readily available data set is at least ten times bigger, but this analysis is currently only focusing on the reduced sample with a blinded strategy to reduced any bias.

This analysis takes advantage of existing tools that have been implemented for the Wire-Cell electron-Low Energy Excess (eLEE) analysis [2], such as the Generic Neutrino Selection (GNS) [3], augmenting these with a BDT-based event selection to improve the current box-cut Wire-Cell NCπ^0 selection and produce the final measurements.

The neutral-current neutral pion channel represents a source of photon background which affects a wide range of measurements, such as the long-baseline neutrino oscillation appearance search ($\nu_\mu \rightarrow \nu_e$) for experiments like DUNE [4], and the single-photon production rate in MicroBooNE. Studying this channel can lead to constraints on such backgrounds to achieve more precise results. The lack of previous NCπ^0 measurements on argon in the sub-GeV to few GeV neutrino energy region (region of interest for MicroBooNE) makes this investigation a priority.

2 Event Selection

2.1 Signal Definition

In this note we measure the interaction defined as

$$\nu_x + Ar \rightarrow \nu_x + \pi^0 + X \tag{1}$$

where ν_x identifies any neutrino or antineutrino, either electron or muon flavor, and X represents the remnant nucleus, any number of neutrons, protons, charged pions and any additional π^0 mesons. This definition doesn't put any requirements on the flavour of the incoming neutrino. A threshold is applied on the true neutrino energy at 275 MeV, motivated as the lowest value in true neutrino energy with a non-zero reconstruction efficiency. No lower bound restriction on the π^0 momentum or angle is required.

2.2 Analysis Input

The event types used in this analysis are summarized in Table 1 and are divided into two categories: data and simulation. The following terms identify the different samples:

- **BNB**: on-beam data;
- **EXTBNB**: a partial set of off-beam data (pure cosmic background) taken during the periods when no beam was received;

- **Overlay Intrinsic** ν_e: simulated neutrino interactions from ν_e present in the beam, overlaid with EXTBNB events;
- **Overlay** ν: simulated neutrino interactions from ν_μ present in the beam, overlaid with EXTBNB events;
- **Dirt**: neutrino interactions happening outside the cryostat.

Since this measurement is currently using a sub-sample of the total data set recorded by the MicroBooNE detector for blinding purposes, the BNB data sample is obtained by merging a fraction of the data recorded during Run 1 ($\sim 4\times10^{19}$ POT) with a fraction of Run 3 ($\sim 1\times10^{19}$ POT). Events from distinct runs, separated in time, allowed the investigation of effects that might not have been present during the early stages of data taking but could have appeared over time. A higher statistical sample includes events from Run 1 to Run 3, and will only be explored after approval of this note. For the simulated samples, a custom tuned version of GENIE was used [5].

Sample	**Type**	**Run**	**POT**
BNB	data	1	4.43×10^{19}
BNB	data	3	9.00×10^{18}
EXTBNB	data	1	2.22×10^{20}
EXTBNB	data	3	7.41×10^{20}
Overlay Intrinsic ν_e	simulation	1	4.00×10^{22}
Overlay Intrinsic ν_e	simulation	3	8.92×10^{22}
Overlay ν	simulation	1	7.30×10^{20}
Overlay ν	simulation	3	7.07×10^{20}
Dirt	simulation	1	1.02×10^{21}
Dirt	simulation	3	1.09×10^{21}

Table 1: Summary of the different data sets used with their corresponding protons-on-target (POT).

The events reported in the plots in this note are labeled as follows:

- **BNB data**: events coming from the BNB samples;
- **EXT**: events coming from the EXTBNB samples, misidentified as the selected neutrino interaction candidate;
- **Dirt**: events coming from the Dirt samples, misidentified as the selected neutrino interaction candidate;
- **Cosmic**: events coming from the Overlay ν and Overlay ν_e samples in which cosmic activity was misidentified as the selected neutrino interaction candidate;
- **NCπ^0 in FV**: non-cosmic true NCπ^0 events coming from the Overlay ν and Overlay Intrinsic ν_e samples with true neutrino vertex inside the fiducial volume (this is the signal);
- **NC in FV**: non-cosmic true NC events without π^0 coming from the Overlay ν and Overlay Intrinsic ν_e samples with true neutrino vertex inside the fiducial volume;

- **ν_eCC in FV**: non-cosmic true ν_eCC events coming from the Overlay ν_e samples with true neutrino vertex inside the fiducial volume;
- **out FV**: non-cosmic events coming from the Overlay ν and Overlay ν_e samples with true neutrino vertex outside the fiducial volume;
- **CCπ^0 in FV**: non-cosmic true ν_μCCπ^0 events coming from the Overlay ν samples with true neutrino vertex inside the fiducial volume;
- **ν_μCC in FV**: non-cosmic truev ν_μCC events without π^0 coming from the Overlay ν samples with true neutrino vertex inside the fiducial volume.

The fiducial volume is defined as the inner volume at 3 cm away from all sides of the effective detector boundaries, corresponding to 94.2% of the full TPC active volume.

2.3 Cosmic Ray Rejection and Generic Neutrino Selection

The MicroBooNE detector operates at the surface, therefore cosmic ray contamination is a serious challenge. After matching reconstructed charge clusters in the TPC with PMT flashes, it is possible to compare the timing given by the flash, which is associated to the charge cluster, to the BNB time windows of 1.6 μs. Rejecting all clusters not in coincidence with the beam enables an increase in the ratio of neutrino interactions to cosmic rays. Through-going muons are successfully tagged by comparing the end points of the clusters with the boundaries of the TPC fiducial volume, while stopped muons, entering from the outside and stopping inside the TPC, are easily labelled by the ionization charge per unit length (dQ/dx) fitting. About 99.98% of the cosmic-ray background events are therefore rejected. This stage is called Generic Neutrino Selection as no specific requirements are placed on the nature of the neutrinos participating in the interactions. Fig. 1 shows the purity as a function of the visible energy in the TPC (defined as the sum of the energies associated to all reconstructed clusters) of the events passing this pre-selection cut. More information can be found in [3].

The Generic Neutrino Selection is implemented as the starting point for the neutral-current π^0 event selection.

2.4 Boosted Decision Tree - Event Selection

A boosted decision tree (BDT) is used to sort neutrino events, with a binary classification, as signal-like and background-like. Several variables are passed to the BDT as input for each event (generally scalar variables) and a single score is obtained as a result of the classification. This analysis makes use of the eXtreme Gradient Boosting (XGBoost) algorithm [6] to implement the BDT.

In order to select the optimal value in the BDT score range that can be used to discriminate signal from background, we investigate the product of efficiency and purity of the validation sample. The maximum of this function is chosen as the cut value of choice.

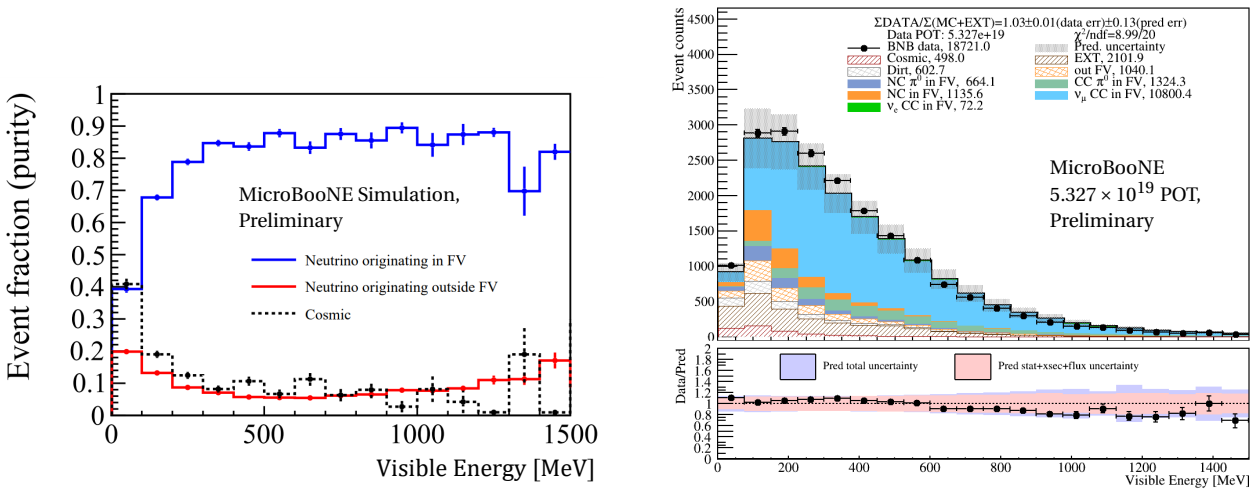

Figure 1: (Left) Event fraction for neutrino-induced and cosmic-ray background events in the selected neutrino candidates. (Right) Selected events passing Generic Neutrino Selection as a function of the visible energy inside the detector.

To summarize the effects of the BDT algorithm, Fig. 2 shows the BDT scores assigned to all events passing the Generic Neutrino Selection. The cut is defined at the BDT score of 1.82.

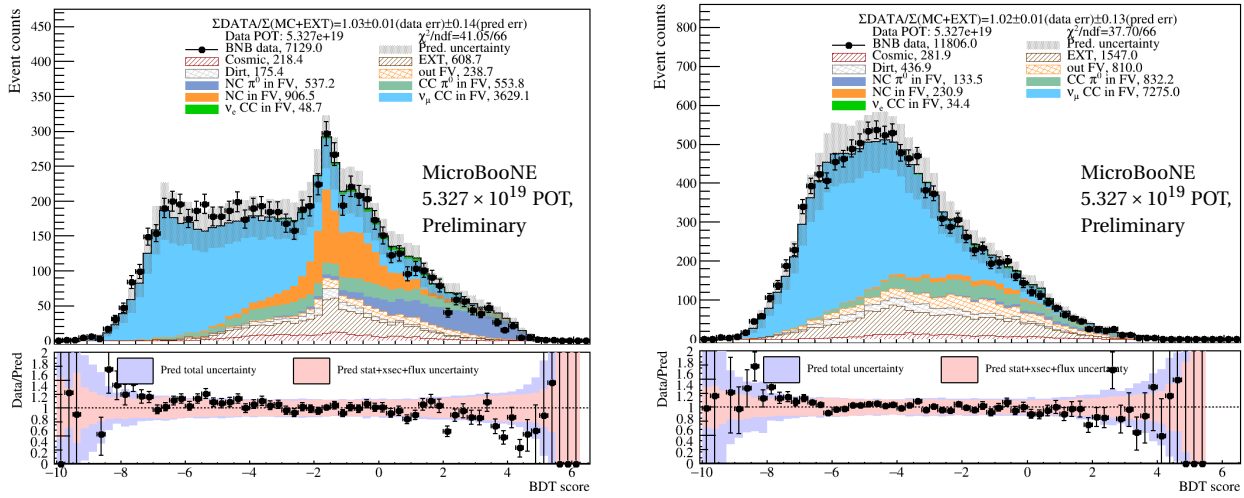

Figure 2: (Left) NCπ^0 BDT score distribution of data and MC after the Generic Neutrino Selection for fully contained events (all reconstructed objects are contained in the TPC active volume, generally referred to as FC), and (Right) for partially contained events (at least one reconstructed object exits the TPC active volume, generally referred to as PC). No events have been excluded by the choice of the range.

3 SYSTEMATIC UNCERTAINTIES

The major systematic uncertainties considered in this analysis can be divided into the following categories:

1. Uncertainties from the Booster Neutrino Beam neutrino flux
2. Uncertainties from neutrino-argon cross sections based on the GENIE event generator

3. Uncertainties from GEANT4 reinteractions between hadrons and argon nuclei
4. Uncertainties from detector performance and effects
5. Uncertainties due to limited Monte Carlo statistics

3.1 Summary of Systematic Uncertainties

The following plots show the summary of the various systematic uncertainties considered in this analysis. The uncertainties are reported for the kinematic distributions with the highest importance for this work for events passing the selection (Fig. 3 and 4). Tables 2 provides additional information to better read and understand the plots. In all plots, the last bin represents the overflow bin. Uncertainties on the number of targets and POT are not shown.

Variable	Range	# of Bins
Corrected visible energy [MeV]	0, 1500	20+1
π^0 Momentum [MeV/c]	0, 1500	25+1
π^0 Mass [MeV/c^2]	0, 300	29+1
π^0 cos θ	-1, 1	20+1

Table 2: Table explaining the bin divisions for Fig. 3, and 4. The number of bins always contains the overflow bin (marked as +1). Systematic uncertainties from POT counting and number of target nuclei are omitted in the plots.

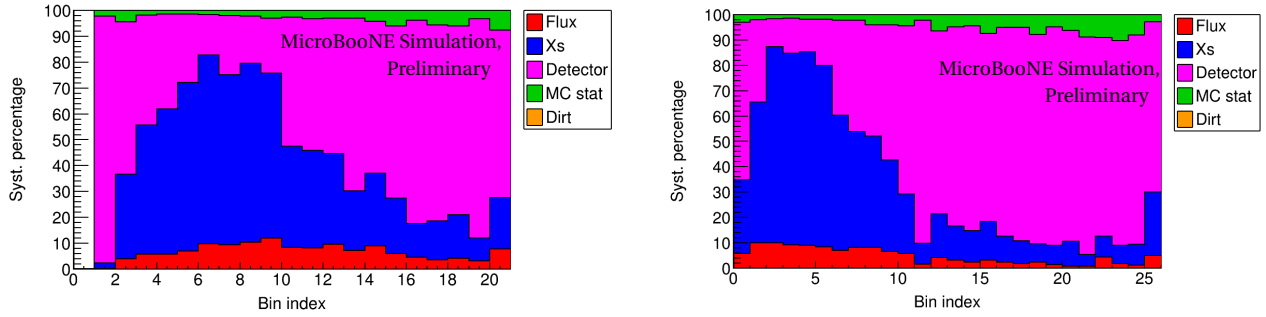

Figure 3: Summary of systematic uncertainties for the corrected visible energy (Left) and the π^0 momentum distributions (Right). The fractional uncertainty defined as $\sigma_i^2/\sigma_{Total}^2 \times 100$ are shown.

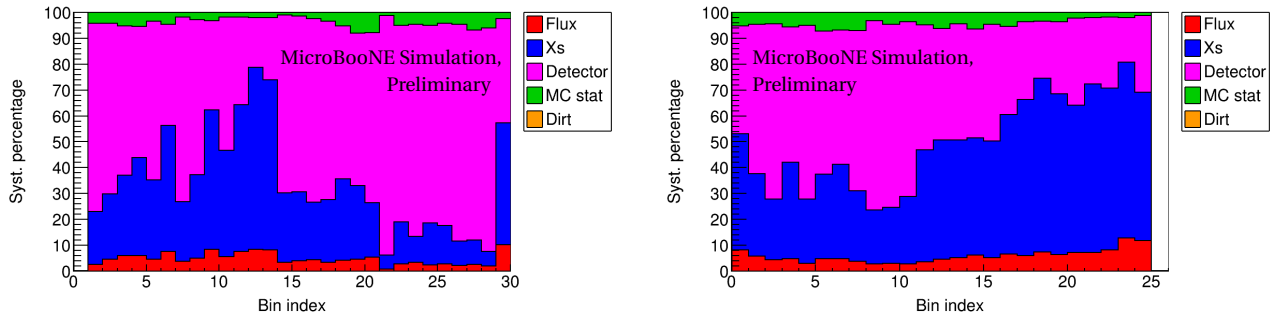

Figure 4: Summary of systematic uncertainties for the π^0 mass (Left) and the π^0 angle distributions (Right). The fractional uncertainty defined as $\sigma_i^2/\sigma_{Total}^2 \times 100$ are shown.

As shown in the fractional uncertainty plots, in bins with high simulation statistics (lower visible energy, lower π^0 momentum, π^0 mass close to the mass peak, and more forward going π^0 angles) the major source of systematic uncertainty seems to be the cross section model, while when the statistics are lower, detector effects seem to play a major role.

4 Open Data Set Results (5.327×10^{19} POT)

Here we report the results of the selection for different kinematic variables, showing the comparison between data and overall prediction for all selected events after applying the cut on the BDT score.

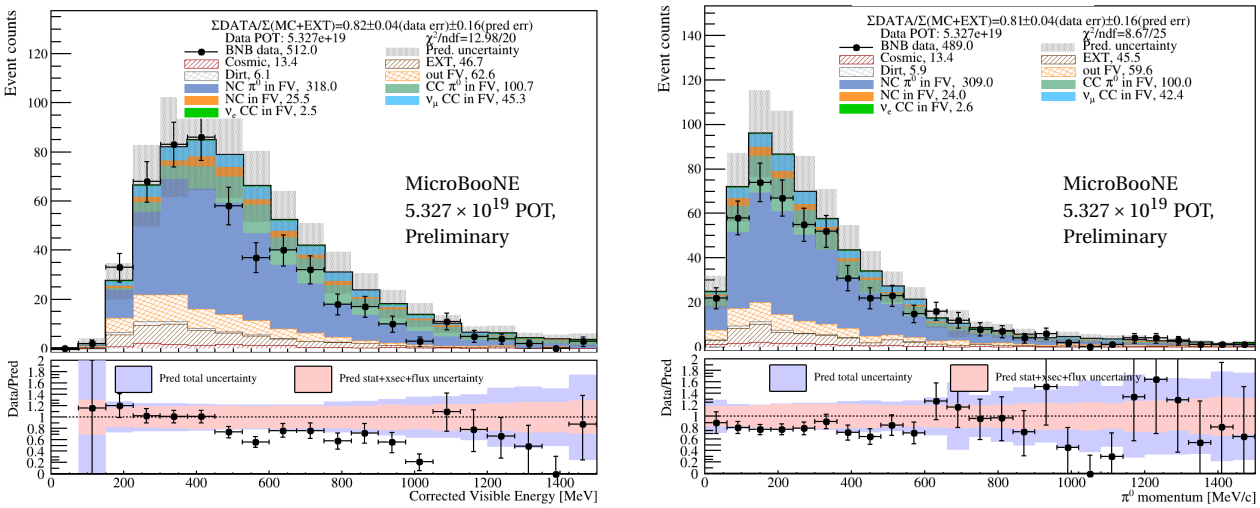

Figure 5: Corrected visible energy (Left) and reconstructed π^0 momentum (Right) for all selected events.

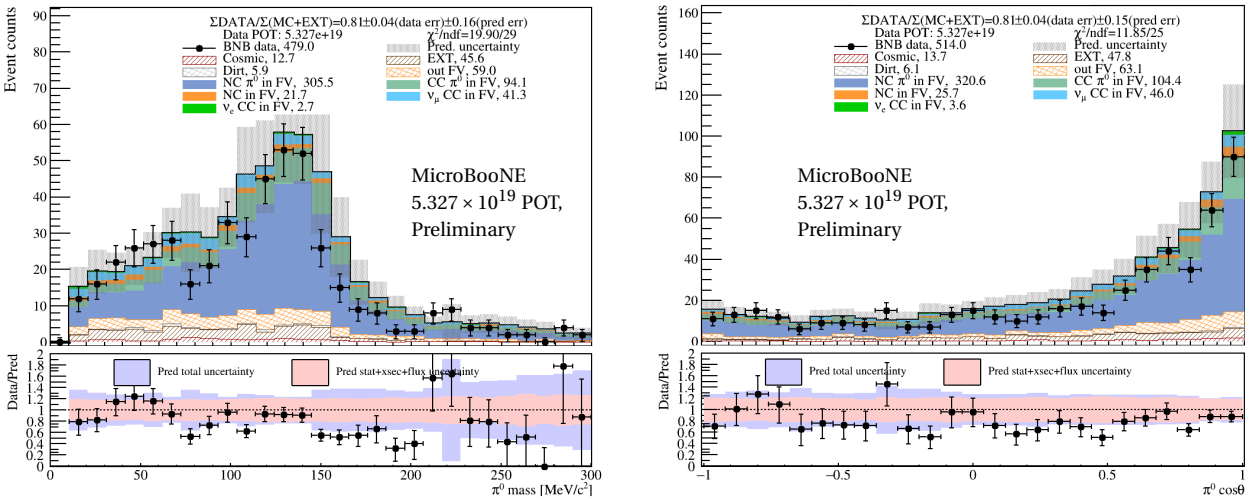

Figure 6: Reconstructed π^0 mass (Left) and reconstructed π^0 angle (Right) for all selected events.

While for all distributions data agrees with the overall predictions within the total uncertainties, a data deficit close to 20% is observed compared to the MC central value. This selection presents a total purity, defined as the ratio of selected true NCπ^0 events to all selected prediction events, of $\sim 51\%$.

Efficiencies as a function of the true neutrino energy, π^0 momentum, and angle are shown below for all selected events and only fully-contained events (Fig. 7). The efficiency is defined as the fraction of selected true NC π^0 events divided by the total number of generated true NC π^0 events with the true vertex in the TPC active volume.

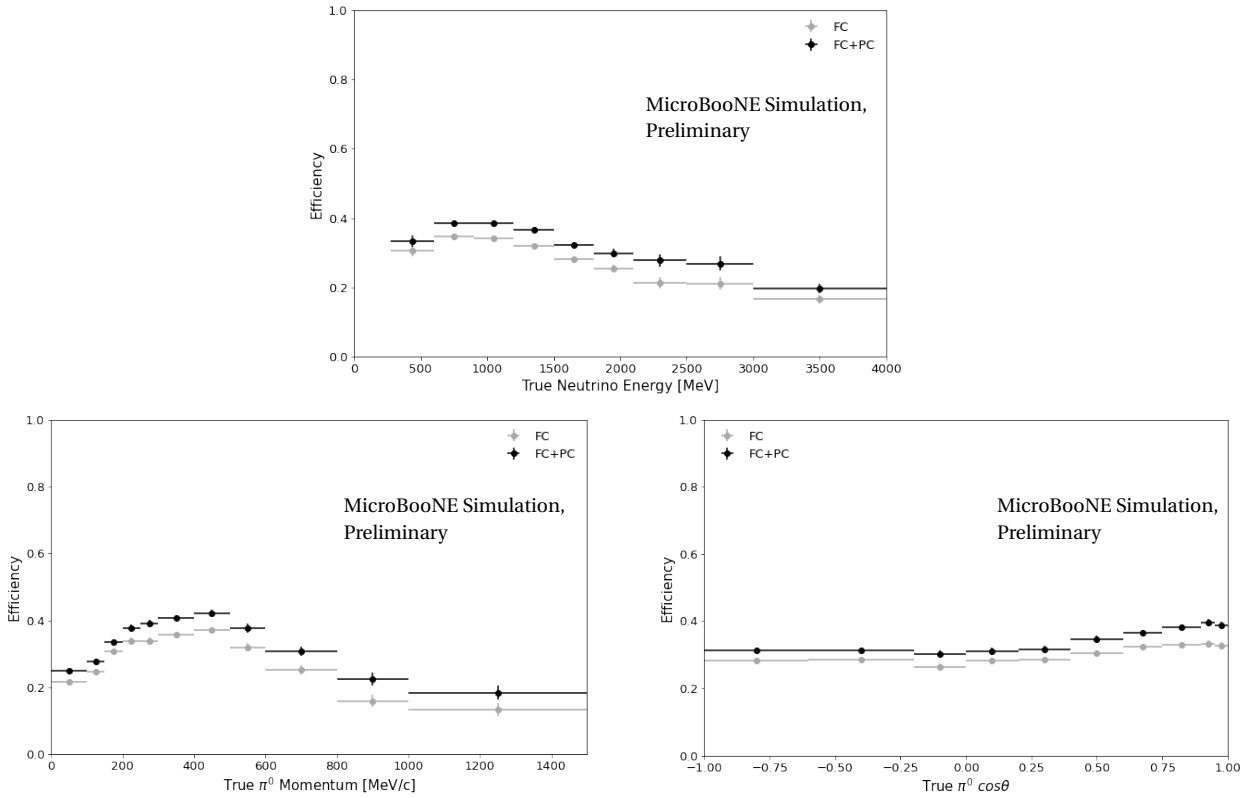

Figure 7: Total efficiency as a function of the true neutrino energy (Top), true π^0 momentum (Bottom Left) and true π^0 angle (Bottom Right) for selected NC π^0 events.

Purity for the selected signal events as a function of the corrected visible energy, π^0 momentum and angle is shown in Fig. 8.

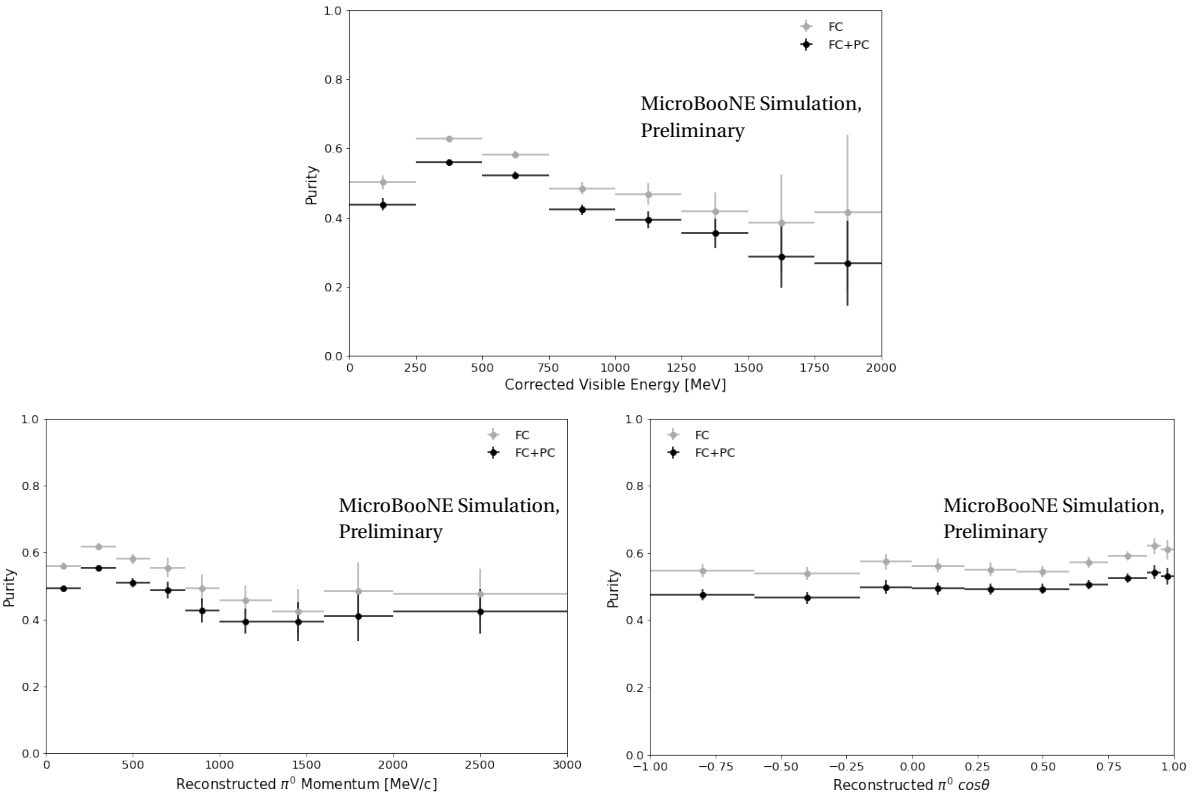

Figure 8: Purity for signal events as a function of the corrected visible energy (Top), reconstructed π^0 momentum (Bottom Left) and reconstructed π^0 angle (Bottom Right) for selected NC π^0 events.

5 Cross Section Results

Flux Calculation

Since not only ν_μ interactions inside the TPC contribute to the final NCπ^0 production, for the following measurements we are considering the flux of all species of neutrino present in the beam (ν_e, $\overline{\nu}_e$, ν_μ, $\overline{\nu}_\mu$), Fig. 9. The sum of these integrated fluxes is used, due to the inability to identify the nature of the incoming neutrino when looking at the final state.

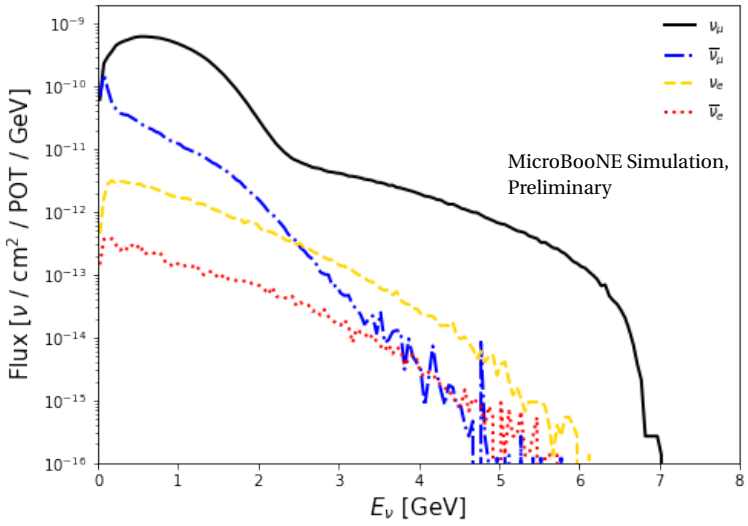

Figure 9: Flux of different neutrino types passing through the LArTPC active volume.

When calculating the flux normalization constant, the neutrino energy range chosen for the total one-bin cross section is also used in the integration of the flux. This means that the area of flux in the range (0, 0.275) GeV is not considered. The integrated flux obtained is therefore

$$\Phi = 3.538 \times 10^9 \nu / cm^2.$$

Number of Targets Calculation

The number of argon atoms in the active volume of the TPC can be calculated using Eq. 2:

$$N = \frac{\rho V N_A}{M_{Ar}} = 1.215 \times 10^{30} \tag{2}$$

with the liquid argon density $\rho = 1.3836$ g/cm^3 in the cryostat, the active volume $V = 5.82515 \times 10^7$ cm^3, the molar mass of argon $M_{Ar} = 39.95$ g/mol, and the Avogadro constant $N_A = 6.022 \times 10^{23}$ mol^{-1}. A relative 1.1% systematic uncertainty is considered on this parameter.

5.1 Total Cross Section Results

Here we report the flux-averaged total one-bin cross section result. Due to the nature of the result, reported as a single bin, there is no need for an unfolding procedure. The total one-bin cross section

is calculated as:

$$\sigma_{NC\pi^0} = \frac{M - B_{MC} - B_{EXTBNB}}{\epsilon\ \Phi\ N} \tag{3}$$

with M being the selected BNB Data, B_{MC} and B_{EXT} the background MC expectation and the selected EXTBNB Data events, ϵ being the efficiency of the selection, Φ the integrated flux, and N the number of targets.

Table 3 summarizes the elements used in the total flux-averaged one-bin cross section extraction, while Fig. 10 reports the measurement and the impact of each uncertainty on the final result.

Targets [10^{30}]	1.215
ν Flux [10^{-10} ν / cm^2 / POT]	6.642
POT [10^{19}]	5.327
Efficiency	0.348 ± 0.003
BNB Data	514.0 ± 22.7
EXTBNB Data	47.8 ± 1.7
Bkg MC	262.6 ± 3.3
Estimated Signal	203.6 ± 23.0
$\sigma_{NC\pi^0}$ [10^{-38} cm^2 / Ar]	$1.43 \pm 0.21 \pm 0.33$

Table 3: Summary table containing the parameters for the cross section calculation. This table reports the statistical uncertainties for the different entries. When not present, only systematic effects are considered. The final cross section measurement is reported in the format $\sigma \pm$ stat $\pm$ sys. For systematic uncertainties see Fig. 10.

Fig. 10 shows a consistent data deficit in the NCπ^0 measurement compared to the GENIE prediction for this measurement, which is also compared to a previous MicroBooNE measurement using the Pandora reconstruction framework [7]. The data deficit is also expected in this cross section measurement given the previously shown distributions in Sec. 4. It is also expected, due to the low statistics of the BNB samples, that statistical uncertainties are dominant in this measurement. Systematics due to the flux and cross section model also contribute strongly to the total uncertainty.

5.2 Differential Cross Section Results

The differential cross section as function of π^0 momentum, extracted using the Wiener-SVD unfolding method [8] in the momentum range between [0-1500] MeV/c, is presented in this section. Fig. 11 shows the covariance matrix and the correlation coefficients in the unfolded π^0 momentum bins; a high correlation is observed for immediately adjacent bins.

The final measurement with the relevant uncertainties is shown in Fig. 12, whereas Table 4 reports the central value and uncertainties for each bin.

The differential cross section shows an over-prediction of the model compared to the data. This is a consistent behavior that we see in the total flux-averaged one-bin cross section measurement

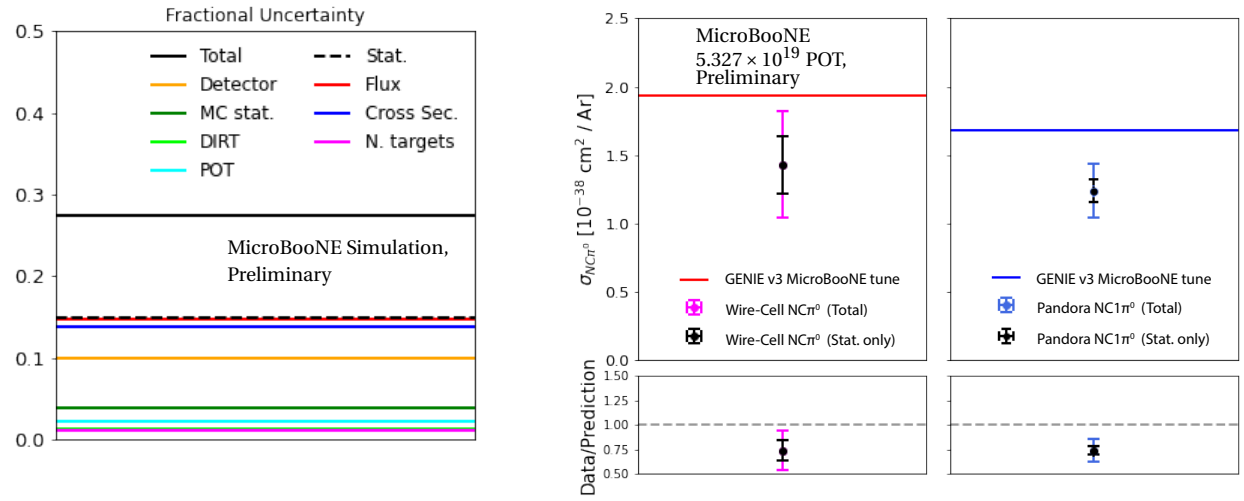

Figure 10: (Left) Fractional uncertainties for the total flux-averaged one-bin cross section. (Right) Final total flux-averaged cross section measurement for 5.327×10^{19} POT. The plot shows two measurements, the first one (WC Inclusive) is the result of this work, and is compared to the GENIE v3 MicroBooNE tune prediction of 1.94 10^{-38} cm^2/Ar (red line). The second measurement (Pandora Semi-inclusive) is the result reported in the Pandora-based analysis for a total POT corresponding to 5.9×10^{20}, [7], which is compared to its GENIE v3 MicroBooNE tune prediction of 1.68 10^{-38} cm^2/Ar (blue line). The signal definitions for the two measurements are slightly different, which accounts for the slightly different GENIE predictions. The comparison demonstrates the consistent data deficit observed by both analyses.

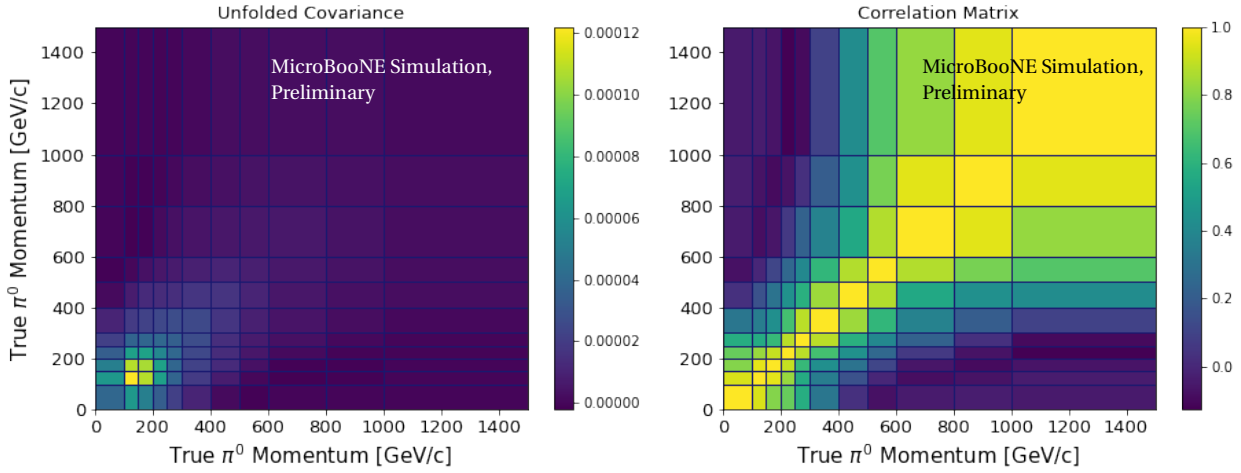

Figure 11: (Left) Covariance matrix, and (Right) correlation coefficient matrix in the unfolded π^0 momentum bins.

as well. As expected, the statistical uncertainty is the dominant source of uncertainty, followed by cross section model and detector systematics.

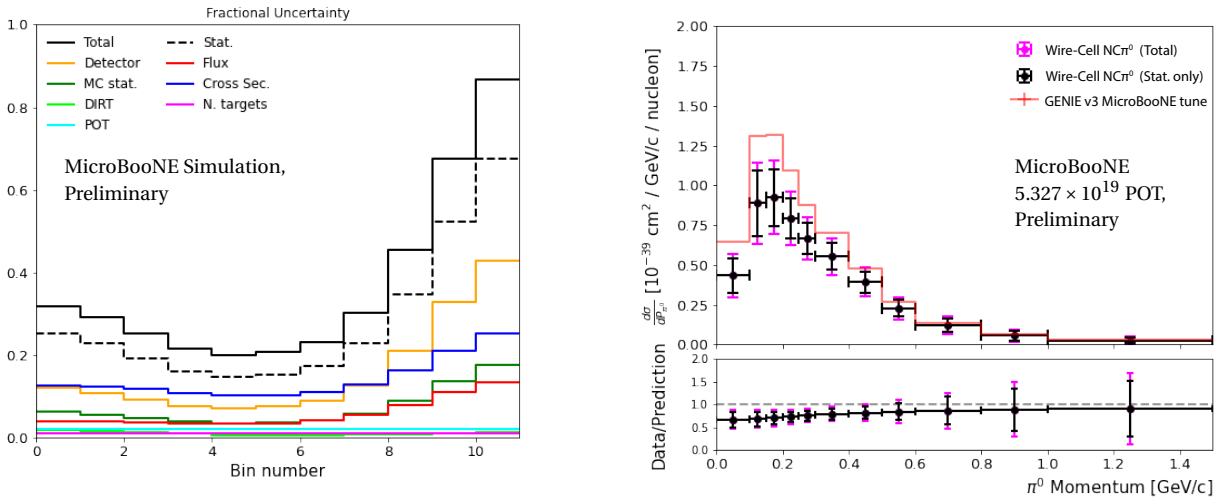

Figure 12: (Left) Fractional uncertainties for the measured differential cross section for each bin, note that systematic uncertainties for POT and number of targets are not shown in the plot, they account respectively for 2.2% and 1.1%. (Right) Differential cross section measurement in true π^0 momentum.

P_{π^0} [GeV/c]	$\frac{d\sigma}{dP_{\pi^0}}$ [10^{-40} cm^2 / GeV/c / nucleon]
(0.00, 0.10)	$4.33 \pm 1.10 \pm 0.83$
(0.10, 0.15)	$8.88 \pm 2.03 \pm 1.59$
(0.15, 0.20)	$9.24 \pm 1.77 \pm 1.48$
(0.20, 0.25)	$7.93 \pm 1.27 \pm 1.13$
(0.25, 0.30)	$6.65 \pm 0.97 \pm 0.90$
(0.30, 0.40)	$5.53 \pm 0.84 \pm 0.76$
(0.40, 0.50)	$3.93 \pm 0.68 \pm 0.60$
(0.50, 0.60)	$2.28 \pm 0.52 \pm 0.45$
(0.60, 0.80)	$1.20 \pm 0.42 \pm 0.35$
(0.80, 1.00)	$0.58 \pm 0.30 \pm 0.25$
(1.00, 1.50)	$0.27 \pm 0.19 \pm 0.15$

Table 4: Tabulated values of the flux-averaged differential cross sections for NCπ^0 production on argon corresponding to the plots in Fig. 12. The values are reported following the format $\sigma \pm$ stat $\pm$ sys.

6 CONCLUSIONS

In conclusion, we have used a relatively pure sample of NCπ^0 events, selected from the available open data set (5.327×10^{19} POT), to produce measurements of total flux-averaged and differential cross sections of NCπ^0 production on argon in MicroBooNE using Wire-Cell. These measurements, which are the principal result of this work, can be found in Fig. 10 and 12 with the respective Tables (3 and 4).

The total flux-averaged cross section has been measured to be $(1.43 \pm 0.21_{stat} \pm 0.33_{sys}) \times 10^{-38}$ cm^2/Ar. These results should provide background constraints to future oscillation experiments as well as single-photon searches in MicroBooNE.

REFERENCES

[1] R. Acciarri et al. (MicroBooNE Collaboration), Design and Construction of the MicroBooNE Detector. *JINST*, 12(02):P02017, 2017.

[2] P. Abratenko et al. (MicroBooNE Collaboration), Search for an anomalous excess of inclusive charged-current ν_e interactions in the MicroBooNE experiment using Wire-Cell reconstruction. *arXiv:2110.13978 [hep-ex]*, [Phys. Rev. D (to be published)].

[3] P. Abratenko et al. (MicroBooNE Collaboration), Cosmic Ray Background Rejection with Wire-Cell LArTPC Event Reconstruction in the MicroBooNE Detector. *Phys. Rev. Applied*, 15(6):064071, 2021.

[4] Babak Abi et al. (DUNE Collaboration), Deep Underground Neutrino Experiment (DUNE), Far Detector Technical Design Report, Volume I Introduction to DUNE. *JINST*, 15(08):T08008, 2020.

[5] C. Andreopoulos et al. The GENIE Neutrino Monte Carlo Generator. *Nucl. Instrum. Meth. A*, 614:87–104, 2010.

[6] Tianqi Chen and Carlos Guestrin. XGBoost: A scalable tree boosting system. In *Proceedings of the 22nd ACM SIGKDD International Conference on Knowledge Discovery and Data Mining*, KDD '16, pages 785–794, New York, NY, USA, 2016. ACM.

[7] P. Abratenko et al. (MicroBooNE Collaboration), Measurement of neutral current single π^0 production on argon with the MicroBooNE detector. *arXiv:2205.07943 [hep-ex]*.

[8] W. Tang, X. Li, X. Qian, H. Wei, and C. Zhang. Data Unfolding with Wiener-SVD Method. *JINST*, 12(10):P10002, 2017.